High Temperature Electrical Resistance of substrate-supported Single Walled Carbon Nanotubes

C. Thomas Avedisian[†a)], Richard E. Cavicchi[‡], Paul M. McEuen[*],

Xinjian Zhou[*], Wilbur S. Hurst[‡] and Joseph T. Hodges[‡]

[†]Sibley School of Mechanical and Aerospace Engineering, Cornell University, Ithaca, New York 14853

[‡]Process Measurements Division, National Institute of Standards and Technology, Gaithersburg, MD. 20899

[*]Department of Physics, Cornell University, Ithaca, New York, 14850

ABSTRACT We report the electrical characteristics of substrate-supported metallic single walled carbon nanotubes (SWNT) at temperatures up to 573 K over a range of bias voltages (V_b) for zero gate voltage in air under atmospheric pressure. Our results show a monotonic increase of resistance with temperature, with an I-V_b characteristic that is linear at high temperature but nonlinear at low temperature. A theory for electrical resistance is applied to the data which shows that the transition to Ohmic behavior at high temperature is the result of optical phonon absorption, rather than acoustic phonon scattering.

[a)]electronic email: cta2@cornell.edu

The electrical characteristics of single walled carbon nanotubes (SWNT) are of interest for a variety of applications, including as transistors and interconnects [1-5], thermal management of electronic systems [6], biological sensors [7], thermal therapeutics for cancer treatment [8] and thermal property measurements [9,10]. In many of the applications a bias voltage (V_b) is imposed across the SWNT at elevated temperatures which makes it important to determine how ambient temperature influences electrical resistance.

A number of studies have reported the measurements of individual SWNTs at temperatures below 300 K [11-17] and fewer studies have reported data at temperatures significantly above 300 K for SWNT ropes, sheets and fibers [1,11,18,19]. Individual *suspended* SWNTs have been taken up to 400 K [5,13,14]. The highest temperature at which the electrical resistance of a nanotube was measured - for a multi-walled carbon nanotube - is 523 K [19].

In this note we report electrical characteristics of individual *substrate-supported* metallic SWNTs over a range of V_b at temperatures up to 573 K in air at atmospheric pressure and for zero gate voltage. Substrate-support provides greater structural integrity than suspended SWNTs; negative differential conductance (NDC) is not generally exhibited because of effective thermal coupling to the substrate and reduced self-heating effects [5,16,20-23]; and contact of a gas with an SWNT can potentially enhance the current carrying capability [13].

SWNTs are obtained by direct growth across FeO_3/MoO_2 catalyst pads placed on a 500 nm SiO_2 layer with a Si substrate in a CVD process under a constant flow of methane as described previously [2,15,22,24,25]. A 50 nm sublayer of Cr lines 10 μm apart is patterned on top of the SiO_2 and a 50 nm Au layer is patterned on top of the Cr. AFM scans showed $L \approx 11 \pm 1$ μm and tube diameters between 1 nm and 2 nm. Devices were electrically probed using an Alessi Rel 4100-A probe station [26] fitted with a Temptronic Thermochuck for heating the tubes. A Keithley 2410 Source Meter was used to obtain two-terminal current-voltage characteristics under LABView control. The electrical characteristics of metallic SWNTs are reported: one tube (SWNT1) is probed up to V_b=2V to potentially promote nonlinear effects; the other tube (SWNT2) is limited to V_b < 0.05V and smaller temperature increments.

Figures 1 and 2 show the measured variation of current with V_b for SWNT1 and SWNT2, respectively, at the indicated temperatures (lines are discussed later).

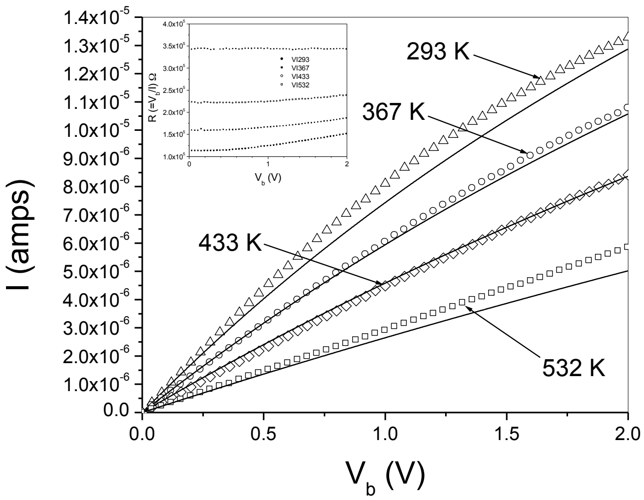

Figure 1

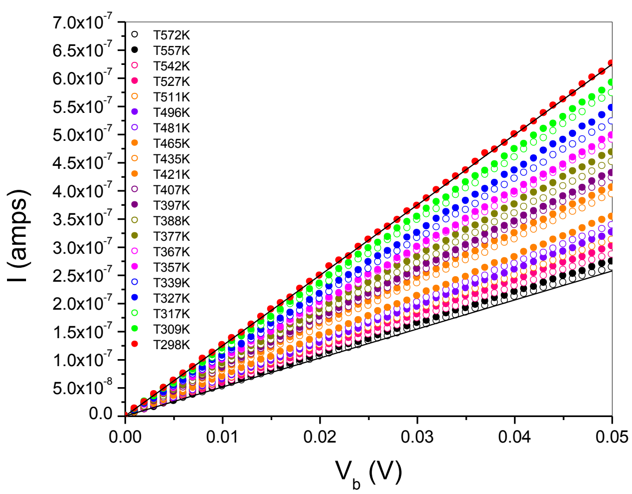

Figure 2

At low bias the variation is linear which means that the resistance ($R = V_b/I$) is independent of V_b (see inset to figure 1). Contact scattering effects [16] are not evident from the data for both of the long SWNTs investigated.

As V_b increases at low temperature for SWNT1, a progressively nonlinear variation of current with

V_b is found, though NDC was not observed. The saturation current for NDC is predicted [16] to be on the order of $I_o \approx \left(4q^2/\hbar\right)h_e$ where $\hbar$, q, and h_e are Planck's constant, electric charge and optical phonon threshold energy, respectively. Taking h_e ~ 0.16 eV (a value associated with zone boundary phonon emission [22]) gives I_o ~ 25μA which is significantly higher than the high bias currents shown in figures 1 and 2.

To understand the temperature effects we apply the Landauer-Buttiker formulation [14]

$$R = R_c + \frac{\hbar}{4q^2}\left[1 + \frac{L}{\lambda_{eff}}\right] \qquad 1$$

with the current determined from $i = \frac{V_b}{R(V_b)}$. In eq. 1, $\hbar$, q, R_c, L and λ_{eff} are Planck's constant, electric charge, contact resistance, SWNT length and total effective mean free path (MFP), respectively, where λ_{eff} includes contributions from acoustic scattering, and optical emission and absorption of phonons:

$$\lambda_{eff} = \frac{1}{\frac{1}{\lambda_{ac}} + \frac{1}{\lambda_{op,ems}} + \frac{1}{\lambda_{op,abs}}} \qquad 2 \quad \text{and}$$

$\lambda_{ac} = \lambda_{aco}\frac{T_o}{T_{ac}}$, $\lambda_{op,abs} = \lambda_{opo}\frac{n_o(T_o)+1}{n_o(T_{op})}$, and $\lambda_{op,ems} = \left(\frac{1}{\lambda_{ems,fld}} + \frac{1}{\lambda_{ems,abs}}\right)^{-1}$. λ_{aco}, λ_{opo} and n_o are the room temperature acoustic scattering MFP, room temperature optical emission MFP, and number of optical phonons, respectively, where $n_o = \left(\exp^{\frac{h_e q}{k_B T_{op}}} -1\right)^{-1}$. T_o is a reference temperature, taken as 300 K, and T_{ac} and T_{op} are phonon temperatures associated with acoustic and optical emission. The contributions to $\lambda_{op,ems}$ come from two effects: the distance (λ_d) required for electrons to reach the energy h_e with the spontaneous optical emission length corrected for temperature, $\lambda_{ems,fld}=\lambda_d+\lambda_{opo}\dfrac{n_o(T_o)+1}{n_o(T_{op})+1}$ where $\lambda_d=L\left(\dfrac{h_e}{q|V_b|}\right)$; and the distance after an optical absorption event [14], $\lambda_{ems,abs}=\lambda_{op,abs}+\lambda_{opo}\dfrac{n_o(T_o)+1}{n_o(T_{op})+1}$.

The approach taken here was to find values of the parameters that best represented the measurements. A simple lumped thermal model for the SWNT temperature is used for the comparatively large aspect ratio (greater than 1000) SWNTs investigated here whereby Joule heating is equated to thermal losses as $i^2(R-R_c)=Lg(T_{ac}-T_\infty)$. g is a measure of the heat loss per unit length to the surroundings, the temperature corresponds to acoustic phonons, and L is the length of the tube. T_{ac} is related to T_{op} as [5,9] $T_{op}=T_{ac}+\alpha(T_{ac}-T_\infty)$ where α is the fraction of the total thermal resistance along the SWNT that is associated with optical phonons.

The STEPIT algorithm [27-29] was used to determine the parameters (R_c, λ_{aco}, λ_{opo}, h_e, α, and g) that globally matched the current and voltage measurements for SWNT1 and SWNT2. The code uses a scheme for sequential examination of trial solutions to find the 'best' that minimizes an objective function, FOBJ, which is defined as $\mathrm{FOBJ}=\sum_{j=1}^{m}\left(\dfrac{i_{j,measured}-i_{j,predicted}}{i_{j,measured}}\right)^2<\varepsilon$ where the index "j" ranges over the individual paired I-V_b measurements and ε is a prescribed error. FOBJ is determined at each step "i" in the search, which includes a strategy for determining variations in parameter step sizes used for the next trial solution. Since the calculation of $T_{ac}(i)$ and $T_{op}(i)$ depends upon adjustable parameters, an internal loop (that rapidly converged) is included to make a consistent calculation. We found that for all of the data reported here, the algorithm always drove g to a "large" value indicating excellent thermal coupling with the substrate and α was driven to zero, the combination of which indicates thermal equilibrium, $T_{op}=T_{ac}=T_\infty$. Furthermore, the best fit (lowest FOBJ) corresponded to R_c being driven to zero as well for all conditions of this study, though from our fabrication process we may in fact expect that $R_c \sim 30\text{k}\Omega$ or less [15]. The extracted room temperature parameters showed little sensitivity to R_c

less than this value. While a precise value of R_c could not be determined, it should be small relative to the measurements shown in figures 3 and 4, especially at high temperature.

For SWNT1 we find that h_e = 0.31 eV, λ_{aco}=650.1 nm, and λ_{opo}=1.04 nm produces the lowest FOBJ. These values are within general expectations except that λ_{opo} is somewhat small compared to previous results [16,22]. The differences appear to be mostly a consequence of the resistance model not describing well the I-V_b characteristics at low temperature (293 K) and high V_b which could be due to additional scattering mechanisms not considered in the model. Figure 3 compares the variation of predicted and measured resistances with temperature for SWNT1. The predicted resistance is a low-bias value taken at V_b = 0.01 V as the inset to figure 1 shows that R does not depend on V_b for V_b < 0.2 V. The experimental resistance values were obtained by linearizing the data (figures 1 and 2) over V_b < 0.05V.

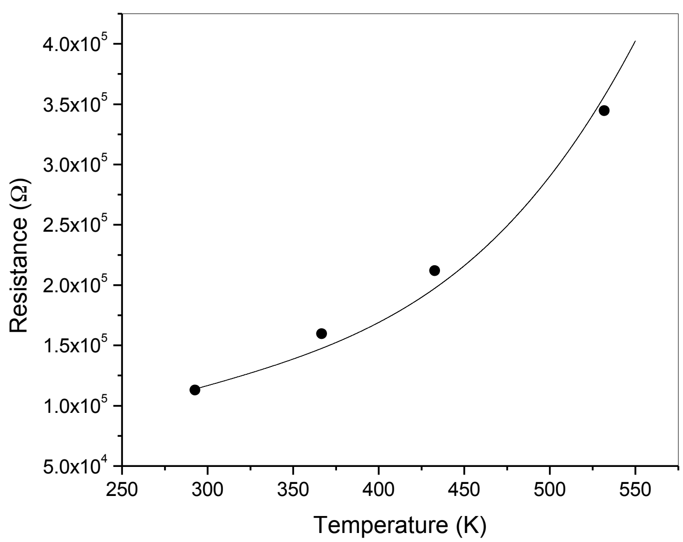

Figure 3

For SWNT2, h_e =0.148 eV, λ_{aco} = 980 nm and and λ_{opo} = 166.1 nm yields the lowest FOBJ. Figure 4 compares the predicted and measured variations of resistance using these parameters.

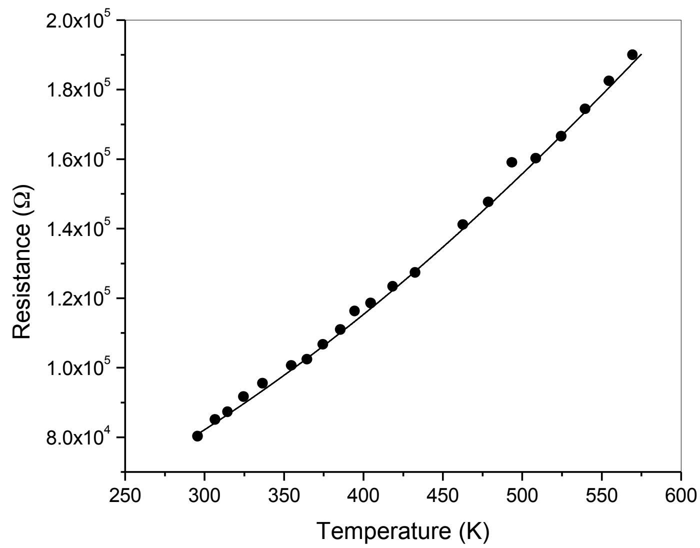

Figure 4

Figures 3 and 4 show resistances that differ by about 25% at low temperature to over 200% at high temperature. Possible reasons include variations of the SWNT chirality which is difficult to control in the manufacturing process, humidity which can influence the relationship between V_b and current [30], or variations in tube diameter (i.e., as $h_e \sim 1/d^2$ [31]). This finding may have a significant impact on using SWNTs in sensing applications as it will require a calibration effort for each SWNT.

To further understand the role of temperature above 300 K and bias on electrical characteristics, figure 5 shows the computed MFPs using the SWNT1 parameters for illustration.

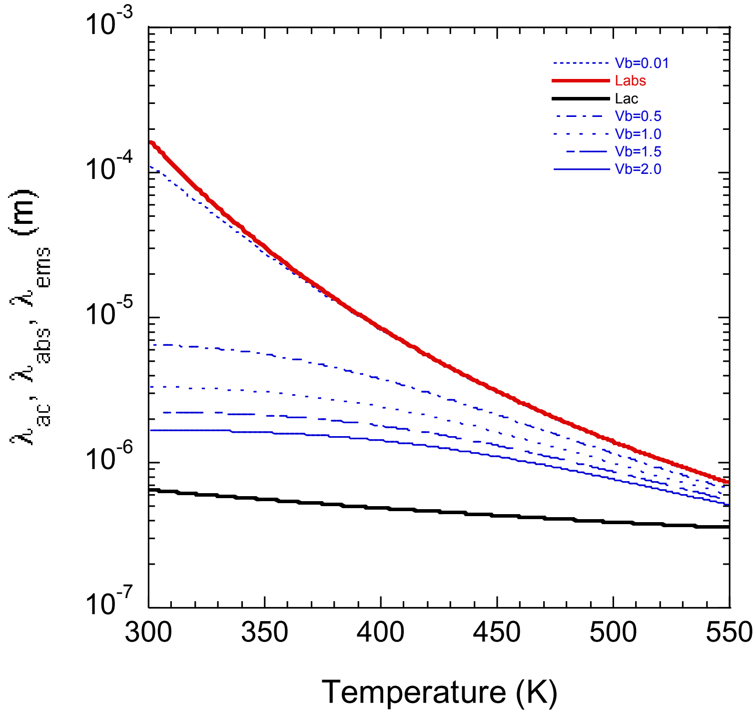

Figure 5

Only the optical emission MFP ($\lambda_{op,ems}$) depends on V_b. At low temperatures (~ 300 K) and low V_b acoustic phonons most influence the flow of current because $\lambda_{ac} << \lambda_{op,ems}$ and $\lambda_{ac} << \lambda_{op,abs}$ so that R (eq. 1) will not then depend on V_b resulting in a linear I-V_b relationship. As V_b increases at low temperature, $\lambda_{op,ems} \sim \lambda_{ac}$ and optical emission phonons which are influenced by V_b begin to exert an influence on current and I is then not linear with V_b. With increasing temperature and a given V_b, $\lambda_{ems,abs} < \lambda_{ems,fld}$ and therefore $\lambda_{op,ems} \sim \lambda_{op,abs}$. It is the $\lambda_{op,abs}$ contribution that produces the strong temperature dependence in $\lambda_{op,ems}$ seen in Figure 5, and this MFP, rather than the weaker temperature dependence of λ_{ac} is responsible for the approach to a linear I-V_b relation observed in the high temperature data in Figure 1.

In summary, we presented data for substrate-supported SWNTs as a function of temperature up to 573K in air and atmospheric pressure. At "low" V_b and "high" temperature both SWNTs show Ohmic behavior though the currents are substantially different at high temperature which yields different room temperature optical and acoustic MFPs that best characterized the data. Reasonable parameter values and good fits to the data are found which indicate excellent thermal coupling to the substrate. The results also show that optical phonon absorption, rather than scattering by acoustic phonons, produces the Ohmic behavior at elevated temperatures.

ACKNOWLEDGMENT. This work was supported in part by the New York State Office of Science, Technology and Academic Research with Dr. Kelvin Lee as the Director. The laboratory assistance of Mr. Johannes Kutten is appreciated. The authors also thank Drs. Casey Mungle, Michael J. Tarlov and John Suehle of NIST for their interest in our work.

Figure Captions

Figure 1: Variation of current with V_b for SWNT1 at four temperatures. Predictions (solid lines) correspond to best-fit values of parameters: λ_{aco}=650.1 nm, $\lambda_{o,o}$= 1.04 nm, $h_e = 0.31\,eV$ and R_c=0.0 Ω.

Figure 2: Variation of current with V_b for SWNT2 at 21 temperatures. Linear correlations shown for 298K and 572K for illustration.

Figure 3: Variation of electrical resistance with temperature for SWNT1. Measured value (•) is obtained by linearizing the measurements (see figure 1) for $0 < V_b < 0.2$V. Predicted resistances correspond to V_b=0.01V and the following parameters: R_c=0.0 Ω, λ_{aco}=650.1 nm, $\lambda_{o,o}$= 1.04 nm and $h_e = 0.31\,eV$.

Figure 4: Variation of electrical resistance with temperature for SWNT2. Measured values (•) are obtained by linearizing the measurements (figure 2) for $0.01 < V_b < 0.05$V. Predicted resistances correspond to V_b=0.01V and the following parameters: λ_{aco}=980 nm, λ_{opo}= 166.1 nm, $h_e = 0.147\,eV$ and R_c=0.0 Ω,.

Figure 5: Variation of MFPs with temperature at various V_b computed using SWNT1 parameters.

References

1. Franklin, N.R., Wang, Q., Tombler, T.W., Javey, A., Shim, M., Dai, H. 2002 Appl. Phys. Lett. 81(5), 913-915.

2. McEuen, P.L., Fuhrer, M.S. and Park, H. 2002 IEEE Trans. Nanotech. 1, 78-85.

3. Javey, A., Guo, J., Wang, Q., Lunstrom, M. and Dai, J. 2003 Nature, 424, 654-657.

4. Kreupl, F., Graham, A.P. Liebau, M., Duesberg, G.S., Seidel, R., Unger, F. 2004 Proc. Int. Electron Devices Meeting (IEDM) paper 29.1, San Francisco.

5. Pop, E., Mann, D., Cao, J., Wang, Q., Goodson, K., Dai, H. 2005 Phys. Rev. Lett. 95, 155505.

6. Hu, X., Padilla, A.A., Xu, J., Fisher, T.S., Goodson, K.E. 2006 J. Heat Transfer, 1109-1113.

7. Besteman, K., Lee, J.O., Wiertz, F.G.M., Heering, H.A. and Dekker, C. 2003 Nano Lett., Vol. 3, No. 6, 727-730.

8. Chakravarty, P., Marches, R., Zimmerman, N.S., Swafford, A.D.E., Bajaj, P., Musselman, I.H., Panton, P., Draper, R.K. and Vitetta, E.S. 2008 Proc. Nat. Acad. Sci. 105(25) 8697-8702.

9. Pop, E., Mann, D., Cao, J., Wang, Q., Goodson, K., Dai, H. 2006 Nano Letters, 6(1), 96-100.

10. Yu, C., Shi, L., Yao, Z. Li, D. and Majumdar, A. 2003 Nano Letters, 5(9), 1842-1846.

11. Kane, C.L., Mele, E.J., Lee, R.S., Fischer, J.E., Petit, P., Dai, H., Thess, A., Smalley, R.E., Verschueren, A.R.M., Tans, S.J., Dekker, C. 1998 Europhys. Lett. 41, 683-688.

12. Fischer, J.E., Dai, H., Thess, A., Lee, R., Hanjani, N.M., Dehaas, D.L. and Smalley, R.E. 1997 Phys. Rev. B. 55, R4921-R4924.

13. Mann, D., Pop, K.E., Cao, J., Wang, Q., Goodson, K. and Dai, H. J. 2006 Phys. Chem. B, 110,

1502-1505.

14. Pop, E., Mann, D., Reifenberg, J., Goodson, K., Dai, H. 2005 paper no. 11.2, Proc. Intl. Electron Devices Meeting (IEDM), Washington, DC.

15. Zhou, X., Park, J.Y., Huang, S., Liu, J. and McEuen, P. L. 2005 Phys. Rev. Lett. 95, 146805.

16. Yao, Z., Kane, C.L. and Dekker, C. 2000 Phys. Rev. Lett. 84, 2941-2944.

17. Mann, D., Javey, A., Kong, J., Wang, Q. and Dai, H. 2003 Nano Lett. 3, 1541-1544.

18. Arai, F., Ng., C., Liu, P., Dong, L., Imaizumi, Y., Maeda, K. Proc. 2004 4th IEEE Conference on Nanotechnology, 146-148.

19. Wei, B.Q., Vajtai, R., and Ajayan, P.M. 2001 Appl. Phys. Lett. 79, 1172-1174.

20. Kuroda, M.A., Cangellaris, A., Leburton, J.P. 2005 Phy. Rev. Lett. 95, 266803.

21. Kuroda, M.A. and Leburton, J.P. 2006 App. Phys. Lett. 89, 103102.

22. Park, J.Y., Rosenblatt, S., Yaish, Y., Sazonova, V., Ustunel, H., Braig, S., Arias, T.A., Brouwer, P.W., and McEuen, P.L. 2004 Nano Lett., 4(3), 517-520.

23. Pop, E., Mann, D., Goodson, K., Dai, H. 2007 J. Appl Phys. 101, 093710.

24. Sazonova, V.A. 2006 "A tunable carbon nanotube resonator," PhD Thesis, Dept. of Physics, Cornell University.

25. V. Sazonova, Y. Yaish, H. Ustunel, D. Roundy, T. A. Arias, and P. L. McEuen, Nature 431, 284 (2004).

26. Certain commercial materials and equipment are identified in order to specify adequately experimental procedures. In no case does such identification imply recommendation or endorsement by

the National Institute of Standards and Technology, nor does it imply that the items identified are necessarily the best available for the purpose.

27. Chandler, J.P. 1975 http://qcpe.chem.indiana.edu/ (enter QCPE code 66)

28. Hooke, R., and Jeeves, T.A. 1961 Journal of the Association for Computing Machinery 8(2) 212-229.

29. Nelder, J.A. and Mead, R. 1975 The Computer Journal 7, 308.

30. Na, P.S., Kim, H., So, H.M., Kong, K.J., Chang, H., Ryu, B.H., Choi, Y., Lee, J.O. Kim, B.K., Kim, J.J., Kim, J. 2005 App. Phys. Lett. 87, 093101.

31 Yamamoto,T., Watanabe, S., and Watanabe, K. 2004 Phys. Rev. Lett. 92, 075502.